

Physical Interaction: Reconstructing Hand-object Interactions with Physics

Haoyu Hu
hhythu17@163.com
School of software and BNRist,
Tsinghua University
China

Xinyu Yi
yixy20@mails.tsinghua.edu.cn
School of software and BNRist,
Tsinghua University
China

Hao Zhang
zhanghao_buaa@163.com
Institute of Computer Application,
China Academy of Engineering
Physics (CAEP)
China

Jun-Hai Yong
yongjh@tsinghua.edu.cn
School of software and BNRist,
Tsinghua University
China

Feng Xu
xufeng2003@gmail.com
School of software and BNRist,
Tsinghua University
China

ABSTRACT

Single view-based reconstruction of hand-object interaction is challenging due to the severe observation missing caused by occlusions. This paper proposes a physics-based method to better solve the ambiguities in the reconstruction. It first proposes a force-based dynamic model of the in-hand object, which not only recovers the unobserved contacts but also solves for plausible contact forces. Next, a confidence-based slide prevention scheme is proposed, which combines both the kinematic confidences and the contact forces to jointly model static and sliding contact motion. Qualitative and quantitative experiments show that the proposed technique reconstructs both physically plausible and more accurate hand-object interaction and estimates plausible contact forces in real-time with a single RGBD sensor.

CCS CONCEPTS

• **Computing methodologies** → **Motion capture.**

KEYWORDS

hand tracking, hand-object interaction, physics-based interaction model, single depth camera

ACM Reference Format:

Haoyu Hu, Xinyu Yi, Hao Zhang, Jun-Hai Yong, and Feng Xu. 2022. Physical Interaction: Reconstructing Hand-object Interactions with Physics. In *SIGGRAPH Asia 2022 Conference Papers (SA '22 Conference Papers)*, December 6–9, 2022, Daegu, Republic of Korea. ACM, New York, NY, USA, 9 pages. <https://doi.org/10.1145/3550469.3555421>

1 INTRODUCTION

In daily lives, humans usually interact with objects with their hands. Thus hand-object interaction is one important kind of motion to be

Permission to make digital or hard copies of part or all of this work for personal or classroom use is granted without fee provided that copies are not made or distributed for profit or commercial advantage and that copies bear this notice and the full citation on the first page. Copyrights for third-party components of this work must be honored. For all other uses, contact the owner/author(s).

SA '22 Conference Papers, December 6–9, 2022, Daegu, Republic of Korea

© 2022 Copyright held by the owner/author(s).

ACM ISBN 978-1-4503-9470-3/22/12.

<https://doi.org/10.1145/3550469.3555421>

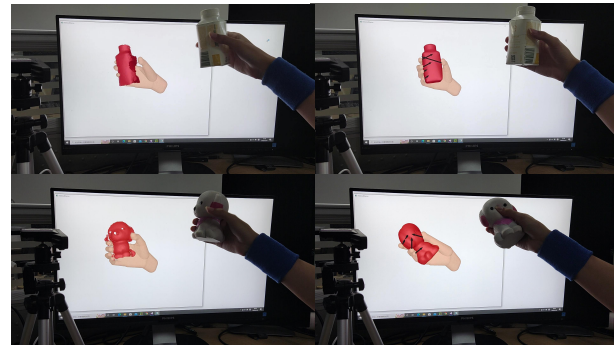


Figure 1: Our system reconstructs physically plausible hand-object interaction and contact forces in real-time from a single-view depth camera.

handled in computer vision and graphics. And reconstructing hand-object interactions is very useful in various applications including gaming, virtual reality, human-computer interaction, and robotics.

Many previous works have worked on the task of reconstructing hand-object interactions. Recently, the state-of-the-art work [Zhang et al. 2021] reconstructs both the hand and the in-hand object in real-time with only a single depth camera. They achieve both promising reconstruction accuracy and runtime performance. However, hand-object interaction usually causes heavy occlusions, leading to severe observation missing, especially in the single view reconstruction scenario. [Zhang et al. 2021] rely on data-driven pose priors to handle this. However, they cannot fully solve the ambiguities, and may fail or generate noticeable artifacts, especially some physically implausible failures and artifacts, *e.g.*, grasping an object with only one finger in contact, or the object slides in the hand, making the technique difficult to be used in many real applications.

These problems motivate us to not only utilize the data-driven priors but also involve physics-driven priors to better solve the ambiguities in the reconstruction. However, it is not trivial to build physical models for hand-object interactions. In body motion capture, we know that physics-based contact and sliding optimizations have been successfully explored [Shimada et al. 2021, 2020; Yi et al.

2022] and are demonstrated useful for realistic human motion estimation. However, different from foot-floor contacts, hand-object contacts are more complicated due to the high freedom of finger motions and the diversity of object shapes. Specifically, 1) hand-object contacts are difficult to detect because of severe occlusions. 2) And modeling the sliding constraints of hand contacts is difficult since fingers can either slide or fix on an object during the interaction.

In this paper, we focus on building a physical model for reconstructing hand-object interactions. We observe that previous works do not delicately model the physics of hand-object interactions. The state-of-the-art work [Zhang et al. 2021] just models the interaction kinematically with only straightforward sliding and penetration constraints, which lacks the awareness of interaction physics. On the other hand, we incorporate delicately designed physics into the traditional kinematic reconstruction of hand-object interaction. First, based on the physical rule that the object’s motion is driven by the forces exerted at the contact points, we propose a novel contact status optimization to iteratively refine the contact status and estimate the contact forces to leverage the object’s dynamics. In this manner, some missing contacts, caused by occlusions, can be recovered by enforcing the consistency between the object motion and the forces on the contacts. Second, with the force estimation, we aim to examine the occurrence of *non-physical sliding* at the contacts, *i.e.*, the contact point falsely slides on the object surface when there is a large pressure on the contact. To deal with false positives caused by the uncertainty in force (pressure) estimation, we design a novel confidence-based slide prevention method, which considers both kinematic confidences and contact forces. With these considerations, we achieve reasonable contact motion estimation, handling both static and sliding contacts. We demonstrate that by incorporating interaction physics into the reconstruction system, we achieve not only physical plausible results but also more accurate hand pose estimation, because the physical priors help to better solve the ambiguities caused by occlusions and noise in the input.

In summary, our main contributions are:

- The first method that reconstructs interacting hand and object with physically plausible contact motions and forces in real-time.
- A physics-based contact status optimization algorithm, which iteratively refines the hand-object contacts leveraging the object dynamics.
- A confidence-based slide prevention algorithm, which eliminates non-physical sliding by incorporating both kinematic confidence and physical force estimation.

2 RELATED WORKS

This paper studies physics-inspired algorithms to improve hand-object interaction reconstruction. So, we majorly review the topics of hand-object interaction reconstruction and physics-based dynamic reconstruction. Notice that there exist numerous methods that focus on pure hand tracking or pure object reconstruction from interacting motions. As they do not simultaneously reconstruct both of them as we do, we will not provide a thorough discussion on them.

2.1 Hand-object Interaction Reconstruction

There are various works aiming at jointly tracking hand pose and object motion during the interaction. Many of them utilize optimization-based methods to find the solutions that best fit the observations which are obtained from different sorts of input. [Ballan et al. 2012; Oikonomidis et al. 2011; Wang et al. 2013] reconstruct hand-object interactions by multi-view RGB cameras, while [Panteleris and Argyros 2017] perform the reconstruction based on stereo RGB cameras. In recent years, depth cameras are widely applied because they can directly provide 3D information. [Kyriazis and Argyros 2014] use RGBD data for motion tracking in complex scenes where the hand interacts with several objects, but the system can only run offline. Real-time performance is achieved by [Sridhar et al. 2016] with RGBD input and a 3D articulated Gaussian mixture alignment approach. All these works need templates of objects in motion estimation, which greatly limits their usage. [Panteleris et al. 2015] track object rigid motions and progressively reconstruct the object shape without a template. Recent works [Zhang et al. 2019, 2021] perform real-time reconstruction of articulated hand pose, object shape, and object rigid/non-rigid motion. Even though they involve data-driven priors to solve the severe ambiguities in the reconstruction, they still suffer from some challenging poses with heavy occlusions. This paper focuses on further providing physics-driven priors to better solve the ambiguity.

Apart from the optimization-based methods, recent works utilize neural networks to extract interaction information directly from single color images. [Tekin et al. 2019] propose a unified network which can simultaneously predict hand-object poses, object categories, and action classes. [Hasson et al. 2019] recover hand and object shapes together with motions through two separate networks. However, for techniques in this category, the generalization ability for novel object geometries is limited because it is difficult to make coverage of the training dataset sufficient, compared to the huge geometry variations in the real world.

2.2 Physics-based Dynamic Reconstruction

Recently, many researches have focused on physics-based dynamic reconstruction. Some works studied physically plausible body motion capture [Li et al. 2019; Rempe et al. 2020; Shimada et al. 2021, 2020; Yi et al. 2022; Zell et al. 2020], character animation and control [Isogawa et al. 2020; Peng et al. 2018a,b; Yu et al. 2021; Yuan and Kitani 2019; Yuan et al. 2021]. Many works focus on physics-based hand motion and hand-object interaction, which are more relevant to our topic. Some works use trajectory optimization [Liu 2009] or data-driven physical controller [Pollard and Zordan 2005; Zhao et al. 2013] to synthesize physics-based dexterous manipulations. Most recent works generate physics-based hand control policy from deep reinforcement learning to reach specific grasping or moving goals [Christen et al. 2022; Yang et al. 2022]. Researches on virtual reality obtain realistic interaction motion by leveraging soft contact modeling and physics simulation [Hirota and Tagawa 2016; Höll et al. 2018; Talvas et al. 2015]. However, these works assume a known virtual object shape and aim at *synthesizing* hand motion to manipulate the object, rather than *hand-object reconstruction*. There are also works focusing on hand-object contact force estimation from visual inputs [Ehsani et al. 2020; Pham et al. 2015,

2017]. They need a good hand-object motion estimation and aim at estimating the real forces during interaction, while we focus on improving the tracking accuracy leveraging physics. Some works explore capturing or refining the hand-object interactive motion leveraging physics [Grady et al. 2021; Kry and Pai 2006; Kumar et al. 2021; Tzionas et al. 2016], which is the most relevant to ours. However, these physical models either have strong assumptions like known object shapes or motion, or are not applicable for the real-time reconstruction task. For the existing physical models of hand-object interaction, there is a gap between effectiveness to solve the ambiguity in the reconstruction task and efficiency to achieve real-time performance.

3 PRELIMINARY

Similar to [Zhang et al. 2021], we use sphere-mesh [Tkach et al. 2016] to model the hand and Truncated Signed Distance Function (TSDF) [Newcombe et al. 2015] to model the object.

Sphere-mesh model deems the human hand as a skeleton that consists of end spheres and connections between spheres. We describe the hand pose with a vector $\theta \in \mathbb{R}^{28}$ that contains 6-DOF wrist pose and 22-DOF finger joint rotations. The object is represented by a static model in zero pose in a canonical space and a motion field consisting of the object’s rigid transformation and non-rigid deformation. The object’s static model is defined as $\mathcal{S} = \{d(\mathbf{x}), w(\mathbf{x})\}$ where \mathbf{x} is a point in the canonical space, $d(\mathbf{x})$ is the signed distance from \mathbf{x} to the closest point on the object surface, and $w(\mathbf{x})$ measures the confidence of $d(\mathbf{x})$. The surface of the static object \mathcal{M} is formulated as:

$$\mathcal{M} = \{(\mathbf{v}, \mathbf{n}) | d(\mathbf{v}) = 0, \mathbf{n} = \frac{\nabla d(\mathbf{v})}{\|\nabla d(\mathbf{v})\|_2}\}, \quad (1)$$

where \mathbf{v} is the vertex and \mathbf{n} is the corresponding normal. The object motion is represented by a motion field $\mathcal{W}(\mathbf{x})$ which is the composition of a rigid transformation \mathbf{W} and a local non-rigid deformation of each vertex. Applying the motion on the static object, we define the live model \mathcal{M}_t as:

$$\mathcal{M}_t = \{(\mathbf{v}_t, \mathbf{n}_t) | \mathbf{v}_t = \mathcal{W}(\mathbf{v})\mathbf{v}, \mathbf{n}_t = \mathcal{W}(\mathbf{v})\mathbf{n}\}. \quad (2)$$

For more details, please refer to [Tkach et al. 2016] and [Newcombe et al. 2015].

4 METHOD

In this section, we present the details of our method. Our task is to reconstruct the interacting hand and object in real-time from a single-view depth camera. The system obtains color and depth image input from the camera and outputs hand pose in terms of joint angles, object motion, and the object 3D model (Fig. 2). Our method incorporates three stages: kinematic hand-object motion tracking (Sec. 4.1), physics-based contact status optimization (Sec. 4.2), and confidence-based contact movement modeling (Sec. 4.3). At the beginning of the motion, we only run the kinematic motion tracking to estimate the object’s static model. After the object is fully reconstructed, we calculate the object’s physical properties and activate the physics-based optimization. As the hand-object contacts can be very dense and complex, it is necessary to simplify the contacts to ensure a stable physics-based optimization and real-time performance. Thus, in this paper, we model the hand-object contacts

only on *fingertips* since they are the most common and important area for hand-object interaction, and suffer from non-physical artifacts (e.g., sliding, penetration, false escape from the object surface) most in previous works. In the following, we elaborate each stage respectively.

4.1 Kinematic Hand-Object Motion Tracking

This stage estimates hand pose θ_{kin}^t , object motion \mathcal{W}^t , and the static object model \mathcal{S} from the input depth map \mathcal{D}^t at frame t . Notice that we use [Zhang et al. 2021] for this kinematic reconstruction step, but in theory, it is applicable for other alternations as our technique is just a refining method working on top of a reconstruction system. Also note that for some symbols that are always associated with frame t , we may eliminate t for simplification.

4.2 Contact Status Optimization

The kinematic motion tracking in Sec. 4.1 suffers from physically incorrect hand-object interaction. In this subsection, we focus on the most important and fundamental part of the interaction, i.e., contacts. Due to the insufficient depth data caused by the single view recording and the hand-object occlusions, we often observe physically implausible contacts in the kinematic tracking results, e.g., the object floats in the air without any finger supporting it. Our idea is to refine the contact status by leveraging the physical prior that the movement of the object should be explained by a group of forces exerted at all contact points. In the following, we introduce the initial contact status extraction and the physics-based contact status refinement.

4.2.1 Initial Contact Status Extraction. As we assume contacts happen on the five fingertips. The contact status can be formulated as:

$$CS = \{(\mathbf{p}_i, \mathbf{n}_i, d_i) | i = 0, 1, \dots, 4\}, \quad (3)$$

where \mathbf{p}_i is the i th fingertip’s projection point on the object surface, \mathbf{n}_i is the normal of the object at \mathbf{p}_i , and d_i is the distance between the tip and \mathbf{p}_i . The projection point \mathbf{p}_i can be treated as the candidate position of the i th fingertip’s contact point on the object surface. d_i somehow represents whether the i th fingertip is in contact with the object ($d_i = 0$ means contact). Here we discuss how to obtain CS . First, we find the candidate contact on the five fingertips. We sample some surface points on each of the fingertip, and based on their positions in the kinematic result, we examine their values in the TSDF of the reconstructed object. The point with minimum values is treated as the candidate as it is the closest to the object. Then we project this point onto the object along the normal direction to get \mathbf{p}_i . And thus \mathbf{n}_i and d_i can also be calculated. Notice that [Zhang et al. 2021] also has a contact detection scheme. It is also applicable to use their method to construct CS .

4.2.2 Physical Properties Calculation. To perform physics-based contact status optimization, we also need to compute the object’s physical properties including dynamics (linear and angular velocity $\mathbf{v}^t, \boldsymbol{\omega}^t$, linear and angular acceleration $\dot{\mathbf{v}}^t, \dot{\boldsymbol{\omega}}^t$) and inherent attributes (mass m_o , center of mass \mathbf{c}_o , and inertia tensor I). The dynamics are derived from previous and current object rigid motion $\{\mathbf{W}^{t-2}, \mathbf{W}^{t-1}, \mathbf{W}^t\}$ using the finite difference method. For the inherent attributes, since mass and its distribution cannot be learned

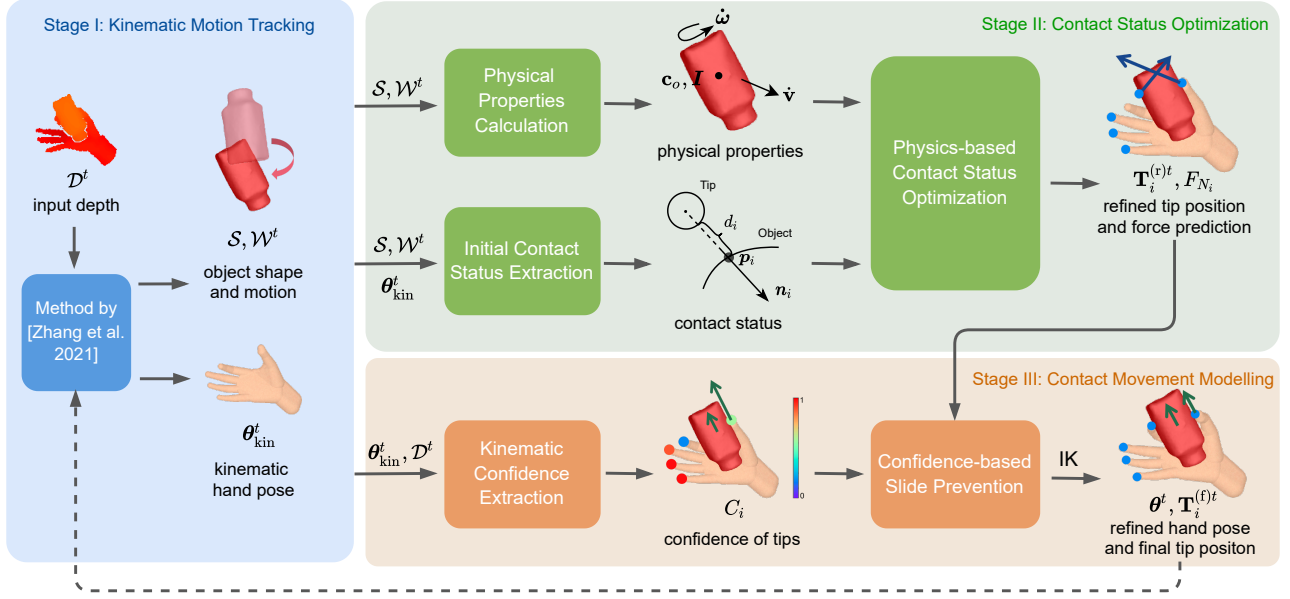


Figure 2: Method overview. We first track the hand-object motion using the method by [Zhang et al. 2021]. Then, we refine the contact status based on the object dynamics. Finally, we model the hand-object movement at the contact points using a confidence-based algorithm. Our physics-based optimization ensures physical plausibility and improves accuracy.

visually, we use a fixed mass $m_o = 0.2\text{kg}$ and assume a hollow object, *i.e.*, mass is evenly distributed on the surface of the object. Note that m_o is just a relative value for solving forces and does not affect the physical refinement. Although not accurate, this simple assumption can work well in preventing the physically implausible failures and artifacts. The center of mass \mathbf{c}_o is the mean position of all vertices on the surface and inertia \mathbf{I} can be computed by:

$$I_{ij} = \frac{m_o}{|\mathcal{M}|} \sum_{k=1}^{|\mathcal{M}|} (\|\mathbf{r}_k\|^2 \delta_{ij} - x_i^{(k)} x_j^{(k)}), \quad i, j \in \{1, 2, 3\}$$

$$\mathbf{r}_k = \mathbf{v}_k - \mathbf{c}_o = (x_1^{(k)}, x_2^{(k)}, x_3^{(k)}), \quad (\mathbf{v}_k, \mathbf{n}_k) \in \mathcal{M}, \quad (4)$$

where δ_{ij} is the Kronecker delta, and I_{ij} is the (i, j) entry of the inertia tensor $\mathbf{I} \in \mathbb{R}^{3 \times 3}$.

4.2.3 Physics-based Contact Status Optimization. This step takes the input of the initial contact status $CS = \{(\mathbf{p}_i, \mathbf{n}_i, d_i)\}$, the object's rigid motion \mathbf{W}^t , and the physical properties $\omega^t, \dot{\mathbf{v}}^t, \dot{\omega}^t, m_o, \mathbf{c}_o, \mathbf{I}$. Our target is to optimize a set of new tip-object distances $\{\tilde{d}_i\}$ which better satisfies the interaction physics. To achieve this, we simultaneously refine the tip-object distances \tilde{d}_i and estimate the force F_i exerted by each tip on the object to explain the object's motion. The intuition behind is that: 1) to explain the object's motion, we must have a set of physically correct forces applied on the object, and 2) based on the condition that a fingertip must *touch* the object to exert force on it, we obtain better contact states by force estimation. Therefore, our optimizer is mathematically defined as:

$$E(\mathbf{f}_i, \tilde{d}_i) = E_f(\mathbf{f}_i) + E_m(\mathbf{f}_i) + E_{\text{reg}}(\mathbf{f}_i) + E_{\text{tac}}(\mathbf{f}_i, \tilde{d}_i) + E_{\text{smo}}(\tilde{d}_i),$$

$$\text{s.t. } \mathbf{f}_i \geq 0, \tilde{d}_i \geq 0. \quad (5)$$

The notation \mathbf{f}_i and each energy term is elaborated in the following.

Tip force modeling. The force F_i , which is exerted by the tip i on the object, is comprised of pressure and friction components which satisfy the Coulomb's Law of Friction. All possible F_i form a friction cone at the contact point \mathbf{p}_i (see Fig. 3). For the tip that is not in contact with the object, we constrain the force in the friction cone centered at the tip-to-object projection point \mathbf{p}_i (though the magnitude of the force can be nearly zero). For computational convenience, we use a polyhedral cone as a linearized approximation of the friction cone. Then, F_i can be expressed by the positive span of four normalized forces at the edges, which we denote as $\mathbf{x}_1, \dots, \mathbf{x}_4$ (see Fig. 3). Let basis matrix $\mathbf{A}_i = [\mathbf{x}_1, \mathbf{x}_2, \mathbf{x}_3, \mathbf{x}_4]$, then the tip force can be computed as $F_i = \mathbf{A}_i \mathbf{f}_i$ ($\mathbf{f}_i \in \mathbb{R}^4, \mathbf{f}_i \geq 0$). To this end, we use \mathbf{f}_i as the optimization variable for the tip forces in Eq. 5, which simplifies the friction cone constraints. The friction coefficient is empirically set to $\mu = 0.7$.

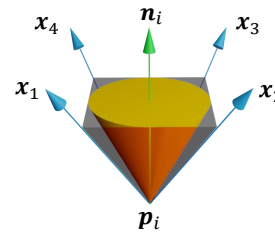


Figure 3: Friction cone (yellow) and its approximation (gray).

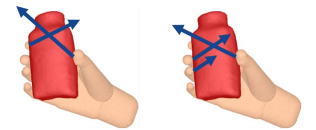


Figure 4: Force ambiguity. Two groups of forces have the same resultant.

Force and moment term. $E_f(\mathbf{f}_i)$ in Eq. 5 requires the object's linear acceleration to be explained by the resultant force including the tip forces and the gravity:

$$E_f(\mathbf{f}_i) = \left\| \sum_{i=0}^4 \mathbf{A}_i \mathbf{f}_i + m_o \mathbf{g} - m_o \dot{\mathbf{v}}^t \right\|^2, \quad (6)$$

where \mathbf{g} is the gravitational acceleration. Similarly, $E_m(\mathbf{f}_i)$ in Eq. 5 requires the object's angular acceleration to be explained by the resultant moment:

$$E_m(\mathbf{f}_i) = \left\| \sum_{i=0}^4 ((\mathbf{p}_i - \mathbf{c}_o^t) \times (\mathbf{A}_i \mathbf{f}_i)) - \boldsymbol{\tau}^t \right\|^2, \quad (7)$$

where $\mathbf{c}_o^t = \mathbf{W}^t \mathbf{c}_o$ is the center of mass of the live object, $\boldsymbol{\tau}^t$ is the driving torque of the object at frame t , which is derived from:

$$\boldsymbol{\tau}^t = \mathbf{I} \dot{\boldsymbol{\omega}}^t + [\boldsymbol{\omega}^t] \mathbf{I} \boldsymbol{\omega}^t, \quad (8)$$

where $[\cdot]$ means the cross product matrix.

Regularization term. We introduce a regularization term $E_{\text{reg}}(\mathbf{f}_i)$ in Eq. 5 to confine the magnitude of the tip forces to be small. This is based on two observations: 1) under specific situations, for example, when two contact points are on the opposite sides and forces are collinear, there are infinite numbers of solutions with arbitrarily large force values. Thus, we need a regularization term to ensure stable force solutions. 2) Humans are used to manipulating objects with the least possible forces. The regularization term is defined as:

$$E_{\text{reg}}(\mathbf{f}_i) = \sum_{i=0}^4 \|\mathbf{f}_i\|^2. \quad (9)$$

Contact term. With the aforementioned terms, a group of forces that best explains the object's movement can be obtained. However, those terms do not model the contacts, *i.e.*, every tip can exert any large forces on the object even if not in contact. Therefore, we introduce the contact term $E_{\text{tac}}(\mathbf{f}_i, \tilde{d}_i)$ in Eq. 5:

$$E_{\text{tac}}(\mathbf{f}_i, \tilde{d}_i) = \sum_{i=0}^4 \|\tilde{d}_i \mathbf{f}_i\|^2, \quad (10)$$

which means a tip can only exert little force (\mathbf{f}_i is small) on the object when it is far from the object surface (\tilde{d}_i is large), and vice versa. This design is simple but important to our system. Originally, updating the contact requires solving a discontinuous optimization at the boundary of contact and not contact. With this design, we formulate it in a continuous optimization without involving noticeable errors. To further constrain the solution, we add another energy term $E_{\text{sno}}(\tilde{d}_i)$ in Eq. 5 to penalize the difference between the optimized contact status and the initial contact status extracted from the kinematic tracking:

$$E_{\text{sno}}(\tilde{d}_i) = \sum_{i=0}^4 (\tilde{d}_i - d_i)^2. \quad (11)$$

4.3 Contact Movement Modeling

With the refined contact status and force estimation, we model the hand-object movement at the contact points in this stage. Since all interaction is done through contacts, correctly modeling the contact movement not only ensures the physical plausibility of the

reconstruction, but also provides movement priors between the object and the hand, which greatly helps us to resolve the ambiguity in the insufficient input data caused by occlusions. Nevertheless, the hand-object movement at the contacts can be very complex: the object can be static, sliding, or rolling at a contact; a soft body can deform at a contact. In our method, we simplify the cases and focus on modeling the most common type of contact movement, *i.e.*, the static and sliding contact.

In the kinematic tracking result, the tip often slides on the object in fast motion when serious blurs exist in the input depth data. Simply forbidding any slip at the contact point will not give a satisfying result. This is because human hands are flexible and can often slide on an object surface when manipulating it. To address this, we propose a physics-based slide prevention method, which utilizes the force predicted in Stage II to constrain the slippage of the contact point with large pressure. This means that the sliding contact is allowed when the pressure is small, which significantly improves the quality and physical plausibility of the interaction. Moreover, the force estimation may be incorrect due to the ambiguities such as multiple contact points as shown in Fig. 4. On the other hand, kinematic tracking may be correct when there is sufficient observation. Considering this, we additionally introduce the tip confidence extracted from the kinematic tracking. In the following, we introduce the confidence extraction and the slide prevention respectively.

4.3.1 Kinematic Confidence Extraction. For each tip, a confidence value C_i is computed from the depth map \mathcal{D}^t and the kinematic tracking results $\boldsymbol{\theta}_{\text{kin}}^t$ based on the number of observed depth points. To be specific, we predefine a number $N_s = 75$ standing for the number of observed depth points that is sufficient for pose estimation of a tip by the kinematic method. Then we check the number of depth points N_i that are close enough (distance smaller than 3mm) to the tip i . Then C_i is defined as:

$$C_i = \min(1, N_i/N_s). \quad (12)$$

Higher confidence indicates that the kinematic tracking gets sufficient data to fit the tip, which yields accurate results. On the contrary, lower confidence means the tip is partly or totally invisible. Leveraging the extracted confidence, our system reduces errors in the physics-based slide prevention, as detailed in the following.

4.3.2 Confidence-based Slide Prevention. The inputs of this module are the five tip positions after the contact status refinement $\mathbf{T}_i^{(r)t} = \mathbf{p}_i + \tilde{d}_i \mathbf{n}_i$, the predicted pressure on each contact point $F_{N_i} = \mathbf{n}_i^T \mathbf{A}_i \mathbf{f}_i$, and the tip confidence C_i . The outputs of this module are the refined tip positions $\mathbf{T}_i^{(s)t}$, which are used in a final inverse kinematics step. We first compute the no-sliding tip positions \mathbf{T}_i^{PS} based on the final tip positions of the previous frame $\mathbf{T}_i^{(f)t-1}$ by:

$$\mathbf{T}_i^{\text{PS}} = \mathbf{T}_i^{(r)t} - (\mathbf{I}_{3 \times 3} - \mathbf{n}_i \mathbf{n}_i^T) (\mathbf{T}_i^{(r)t} - \mathbf{W}^t (\mathbf{W}^{t-1})^{-1} \mathbf{T}_i^{(f)t-1}), \quad (13)$$

where $\mathbf{I}_{3 \times 3}$ is an identity matrix, $\mathbf{I}_{3 \times 3} - \mathbf{n}_i \mathbf{n}_i^T$ stands for a tangential projection on a surface point with the normal \mathbf{n}_i , \mathbf{W}^t and \mathbf{W}^{t-1} are the object poses at the current and the last frame, respectively. In this way, the obtained \mathbf{T}_i^{PS} has the same contact point as the previous frame but possible rigid and nonrigid deformation is allowed

Table 1: Quantitative evaluation of different solutions using average pixel errors of all five fingertips in all frames.

	bl	cso	cso+fri	cso+fri+conf
Average Pixel Error	11.58	10.22	11.20	9.67

for the object. Then, we compute the refined tip positions $T_i^{(s)t}$ as:

$$T_i^{(s)t} = \begin{cases} T_i^{(r)t} & F_{N_i} < \alpha G_o \\ T_i^{PS} & F_{N_i} \geq \alpha G_o \text{ and} \\ & C_i \leq \frac{\beta}{\|T_i^{(r)t} - T_i^{PS}\|} \\ \gamma T_i^{(r)t} + (1 - \gamma) T_i^{PS} & \text{otherwise} \end{cases}, \quad (14)$$

where $G_o = m_o \|g\|$ is the object’s gravity, α is a fixed scale parameter, β is used to control the effect of the confidence C_i , and γ is used to smooth the sliding process. We empirically set $\alpha = 0.3$, $\beta = 5\text{mm}$, $\gamma = 0.5$. We use a mass-dependent threshold αG_o to determine whether a tip can slide since the pressure F_{N_i} solved in Stage II is proportional to m_o . When sliding is allowed physically (the pressure is small, *i.e.*, $F_{N_i} < \alpha G_o$ in Eq. 14), we merely output the result $T_i^{(r)t}$ from the previous stage. Otherwise, the tip movement along the contact tangential is restricted based on the kinematic confidence of the tip C_i . With low confidence, we tend to believe that the slide is caused by the tracking error, hence choose to prevent slippage (the middle row in Eq. 14). Otherwise, we choose to slide and perform a linear interpolation to smooth this process (the last row in Eq. 14). We use a dynamic threshold for confidence-based slide judgement. This is because even under fully observation ($C_i = 1$), slippage is still inevitable in the kinematic result but only with small errors.

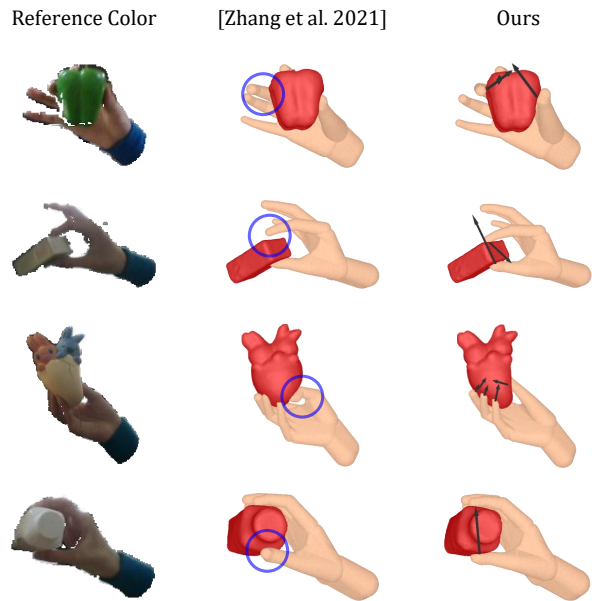
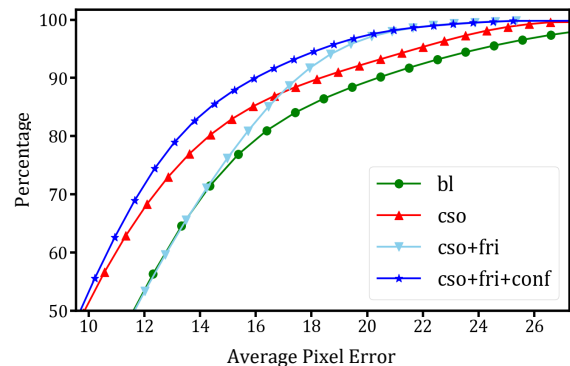
Finally, we perform inverse kinematics to obtain the final hand pose θ^t using the refined tip positions $T_i^{(s)t}$. We also calculate the final tip positions $T_i^{(f)t}$ from θ^t , which are used in the next slide prevention stage of the next frame.

5 EXPERIMENTS

In this section, we first provide the experimental settings of our system. Then, we compare our method with the state-of-the-art work [Zhang et al. 2021] and evaluate the effectiveness of our key techniques qualitatively and quantitatively. Finally, we discuss our limitations. More results of rigid and nonrigid object motions of various object shapes, sizes, and textures are shown in Fig. 1 and the supplementary video.

5.1 Experimental Settings

We use one RealSense SR300 sensor to record the depth stream of hand-object interactions with the resolution of 320×240 . Two NVIDIA TITANXp GPUs are used for the network evaluation and energy optimization respectively in the kinematic tracking stage. The physical refinement stage purely runs on an AMD Ryzen 5700g CPU. The contact status optimization Eq. 5 is solved by the LM algorithm [Moré 1978]. Our system can process one frame within 40ms, where 32ms for kinematic tracking and 8ms for physical refinement.

**Figure 5: Qualitative comparison with [Zhang et al. 2021].****Figure 6: Percentage of correct hand tips. It stands for better performance if the curve is closer to the top-left corner.****Table 2: Proportion of physically implausible frames (less than 2 contacts).**

	[Zhang et al. 2021]	Ours
Implausible Ratio (%)	54.7	2.0

5.2 Comparisons

Our work uses [Zhang et al. 2021] for kinematic tracking which is also the state-of-the-art in this topic, so we compare our system with it to demonstrate the effectiveness of our physics-based refinement on precision and physical plausibility. The qualitative results are shown in the supplementary video and Fig. 5. In the top two rows of Fig. 5, we can clearly see that sometimes a contact may not be discovered by [Zhang et al. 2021] while we correctly reconstruct

it by the physics-based contact status optimization. Meanwhile, in the bottom two rows of Fig. 5, some contacts may slide to a wrong position in the result of [Zhang et al. 2021] due to the lack of observation. While in our result, as we model the friction, the contact position is better preserved. Note that our method can prevent error accumulation in the kinematic tracking system (e.g., the third row in Fig. 5). This is because the hand pose solved in the previous frame is used to initialize the next frame. Thus, the physical refinement can influence the solution in the subsequent frames. More visual comparisons can be found in the supplementary video.

For a quantitative comparison on precision, we use the same metric as [Zhang et al. 2021]. We project five fingertips of the reconstruction result onto the RGB camera and manually label the tips on the color images as ground truth. The average pixel error is used to measure the accuracy of hand tracking. We prepare three annotated sequences for this comparison: "MoveBox" with 480 frames, "RotateBottle" with 390 frames, and "HandleToy" with 550 frames. Tab. 1 shows the values of average pixel errors on the three recorded sequences and Fig. 6 reports the corresponding aggregated errors. *bl* stands for our kinematic tracking result which is just the result of [Zhang et al. 2021]. These comparisons further demonstrate that our method can improve the tracking accuracy of fingertips and lessen the maximum error as the curve in Fig. 6 is more on the left.

To demonstrate that our results are more physically plausible, we compute the ratio of frames with less than two contact points in the aforementioned three sequences. As multiple contact points are necessary for supporting an object in most cases, we regard circumstances violating this as physically implausible. Tab. 2 shows that our method can significantly reduce the implausible cases by adding sufficient contact points based on our physical model.

5.3 Evaluation

We first quantitatively evaluate the effectiveness of the key components in our physical refinement, which is also shown in Tab. 1 and Fig. 6. Here we show the results of four solutions, pure kinematic results (*bl*), contact status optimization only (*cso*), contact status optimization + pure friction-based slide prevention (*cso+fri*), and contact status optimization + confidence-based slide prevention (*cso+fri+conf*). Contact status optimization (*cso*) helps to resolve the problem that fingertips fail to properly contact the object and it reduces the numerical errors noticeably. However, adding the friction-based sliding prevention (*cso+fri*) cannot further reduce the errors but increase them a little bit. This is because this module is purely based on physics without considering the kinematic information. If the initial contact position has errors, fixing its position by friction makes the contact position impossible to be refined, leading to worse results sometimes. As in the case with strong observations, kinematic results are usually correct. So, after adding the kinematic-involved confidence component (*cso+fri+conf*), the errors dropped and the best performance in this experiment is achieved.

We also show some qualitative results here. In Fig. 7, we see that the kinematic reconstruction fails to reconstruct the left contact point due to the relatively fast motion. The index finger wrongly fits the observation of the middle finger and moves wrongly with the

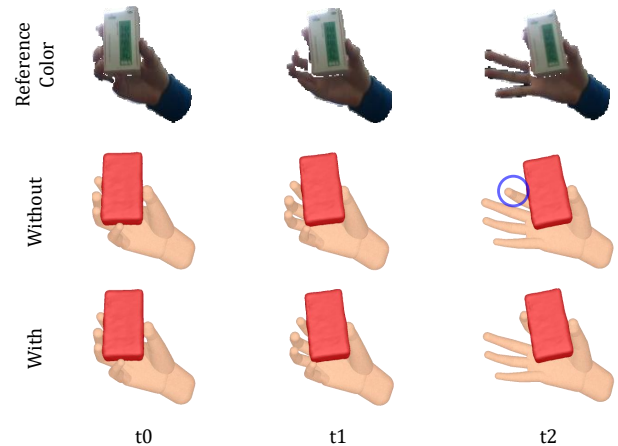


Figure 7: Qualitative evaluation of our contact status optimization.

middle finger. On the other hand, *cso* knows that one contact cannot prevent the object from falling down and correctly discovers the second contact point. More results are shown in the supplementary video. Fig. 8 gives one visual example to show the effectiveness of our confidence-based slide prevention. In these snapshots of a short sequence, we see that without this slide prevention, the thumb wrongly slides on the object surface due to the lack of observations when the object turns at frames around t_1 and t_2 . Notice that the involvement of kinematic confidence not only fixes the contact when pressure exists, but also allows sliding when no pressure exists. To better demonstrate this, we show the result in the supplementary video in the section "Evaluation of the Confidence".

5.4 Limitations

To guarantee real-time performance, our physical model is largely simplified and thus still far from real physics. First, we assume the contacts only happens on fingertips. For cases breaking this assumption, our system goes back to a kinematic tracking system. Second, we solve for the contact forces with assumptions on object masses. This may lead to inaccurate contact force magnitudes, but still successfully brings physical plausibility into the reconstruction system. Third, when tracking non-rigid objects, we fix inertia information instead of updating it with the object's deformation. In most cases, this only affects the accuracy of the force solution. However, for strong deformations, this simplification may lead to wrong contact positions due to the big errors in the physical properties.

6 CONCLUSIONS

This paper proposes a physical method for modeling the complex motion of hand-object interaction and demonstrates its power in single view real-time reconstruction. The method first models the relationship between the contact forces and the dynamics of the in-hand object, which is successfully used in recovering unobserved contacts as well as the contact forces. It also jointly models the static and sliding contact motions, which are used to reconstruct accurate contact motions by combining both the kinematic confidence and

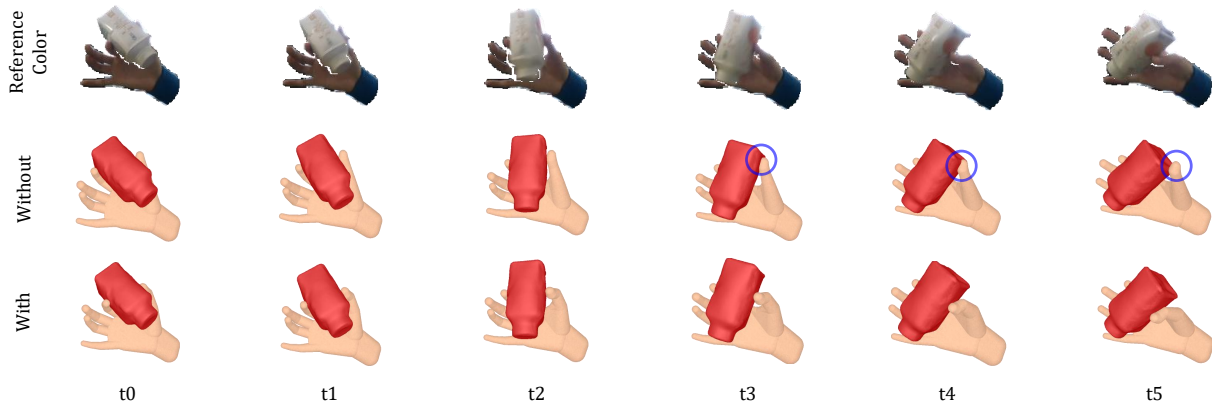


Figure 8: Qualitative evaluation of our slide prevention in a sequence.

the contact forces. In general, this technique achieves physically plausible and more accurate interaction reconstruction in real-time using a single view input, with a byproduct of plausible forces.

ACKNOWLEDGMENTS

This work was supported by Beijing Natural Science Foundation (JQ19015), the NSFC (No.62021002, 61727808), the National Key R&D Program of China 2018YFA0704000, the Key Research and Development Project of Tibet Autonomous Region XZ202101ZY0019G. This work was supported by THUIBCS, Tsinghua University and BLBCI, Beijing Municipal Education Commission. Feng Xu and Jun-Hai Yong are the corresponding authors. Hao Zhang contributed to this work when he was a PhD student in Tsinghua University.

REFERENCES

- Luca Ballan, Aparna Taneja, Jürgen Gall, Luc Van Gool, and Marc Pollefeys. 2012. Motion capture of hands in action using discriminative salient points. In *European Conference on Computer Vision*. Springer, 640–653.
- Sammy Christen, Muhammed Kocabas, Emre Aksan, Jemin Hwangbo, Jie Song, and Otmar Hilliges. 2022. D-Grasp: Physically Plausible Dynamic Grasp Synthesis for Hand-Object Interactions. In *Proceedings of the IEEE/CVF Conference on Computer Vision and Pattern Recognition*. 20577–20586.
- Kiana Ehsani, Shubham Tulsiani, Saurabh Gupta, Ali Farhadi, and Abhinav Gupta. 2020. Use the force, luke! learning to predict physical forces by simulating effects. In *Proceedings of the IEEE/CVF Conference on Computer Vision and Pattern Recognition*. 224–233.
- Patrick Grady, Chengcheng Tang, Christopher D Twigg, Minh Vo, Samarth Brahmabhatt, and Charles C Kemp. 2021. Contactopt: Optimizing contact to improve grasps. In *Proceedings of the IEEE/CVF Conference on Computer Vision and Pattern Recognition*. 1471–1481.
- Yana Hasson, Gul Varol, Dimitrios Tzionas, Igor Kalevtykh, Michael J Black, Ivan Laptev, and Cordelia Schmid. 2019. Learning joint reconstruction of hands and manipulated objects. In *Proceedings of the IEEE/CVF conference on computer vision and pattern recognition*. 11807–11816.
- Koichi Hirota and Kazuyoshi Tagawa. 2016. Interaction with virtual object using deformable hand. In *2016 IEEE Virtual Reality (VR)*. IEEE, 49–56.
- Markus Höll, Markus Oberweger, Clemens Arth, and Vincent Lepetit. 2018. Efficient physics-based implementation for realistic hand-object interaction in virtual reality. In *2018 IEEE Conference on Virtual Reality and 3D User Interfaces (VR)*. IEEE, 175–182.
- Mariko Isogawa, Ye Yuan, Matthew O’Toole, and Kris Kitani. 2020. Optical Non-Line-of-Sight Physics-Based 3D Human Pose Estimation. In *2020 IEEE/CVF Conference on Computer Vision and Pattern Recognition (CVPR)*.
- Paul G Kry and Dinesh K Pai. 2006. Interaction capture and synthesis. *ACM Transactions on Graphics (TOG)* 25, 3 (2006), 872–880.
- Akarsh Kumar, Aditya R Vaidya, and Alexander G Huth. 2021. Physically Plausible Pose Refinement using Fully Differentiable Forces. *arXiv preprint arXiv:2105.08196* (2021).
- Nikolaos Kyriazis and Antonis Argyros. 2014. Scalable 3d tracking of multiple interacting objects. In *Proceedings of the IEEE Conference on Computer Vision and Pattern Recognition*. 3430–3437.
- Zongmian Li, Jiri Sedlar, Justin Carpentier, Ivan Laptev, Nicolas Mansard, and Josef Sivic. 2019. Estimating 3D Motion and Forces of Person-Object Interactions from Monocular Video. In *Computer Vision and Pattern Recognition (CVPR)*.
- C Karen Liu. 2009. Dexterous manipulation from a grasping pose. In *ACM SIGGRAPH 2009 papers*. 1–6.
- Jorge J Moré. 1978. The Levenberg-Marquardt algorithm: implementation and theory. In *Numerical analysis*. Springer, 105–116.
- Richard A Newcombe, Dieter Fox, and Steven M Seitz. 2015. Dynamicfusion: Reconstruction and tracking of non-rigid scenes in real-time. In *Proceedings of the IEEE conference on computer vision and pattern recognition*. 343–352.
- Iason Oikonomidis, Nikolaos Kyriazis, and Antonis A Argyros. 2011. Full dof tracking of a hand interacting with an object by modeling occlusions and physical constraints. In *2011 International Conference on Computer Vision*. IEEE, 2088–2095.
- Paschalis Panteleris and Antonis Argyros. 2017. Back to rgb: 3d tracking of hands and hand-object interactions based on short-baseline stereo. In *Proceedings of the IEEE International Conference on Computer Vision Workshops*. 575–584.
- Paschalis Panteleris, Nikolaos Kyriazis, and Antonis A. Argyros. 2015. 3D Tracking of Human Hands in Interaction with Unknown Objects. In *Proceedings of the British Machine Vision Conference (BMVC)*. Article 123, 12 pages.
- Xue Bin Peng, Pieter Abbeel, Sergey Levine, and Michiel van de Panne. 2018a. DeepMimic: Example-Guided Deep Reinforcement Learning of Physics-Based Character Skills. *ACM Trans. Graph.* 37 (jul 2018).
- Xue Bin Peng, Angjoo Kanazawa, Jitendra Malik, Pieter Abbeel, and Sergey Levine. 2018b. SFV: Reinforcement Learning of Physical Skills from Videos. *ACM Trans. Graph.* 37 (nov 2018).
- Tu-Hoa Pham, Abderrahmane Kheddar, Ammar Qammar, and Antonis A Argyros. 2015. Towards force sensing from vision: Observing hand-object interactions to infer manipulation forces. In *Proceedings of the IEEE conference on computer vision and pattern recognition*. 2810–2819.
- Tu-Hoa Pham, Nikolaos Kyriazis, Antonis A Argyros, and Abderrahmane Kheddar. 2017. Hand-object contact force estimation from markerless visual tracking. *IEEE transactions on pattern analysis and machine intelligence* 40, 12 (2017), 2883–2896.
- Nancy S Pollard and Victor Brian Zordan. 2005. Physically based grasping control from example. In *Proceedings of the 2005 ACM SIGGRAPH/Eurographics symposium on Computer animation*. 311–318.
- Davis Rempe, Leonidas J. Guibas, Aaron Hertzmann, Bryan Russell, Ruben Villegas, and Jimei Yang. 2020. Contact and Human Dynamics from Monocular Video. In *Proceedings of the European Conference on Computer Vision (ECCV)*.
- Soshi Shimada, Vladislav Golyanik, Weipeng Xu, Patrick Pérez, and Christian Theobalt. 2021. Neural Monocular 3D Human Motion Capture with Physical Awareness. *ACM Transactions on Graphics* 40 (aug 2021).
- Soshi Shimada, Vladislav Golyanik, Weipeng Xu, and Christian Theobalt. 2020. PhysCap: physically plausible monocular 3D motion capture in real time. *ACM Transactions on Graphics* 39 (dec 2020).
- Srinath Sridhar, Franziska Mueller, Michael Zollhöfer, Dan Casas, Antti Oulasvirta, and Christian Theobalt. 2016. Real-time joint tracking of a hand manipulating an object from rgb-d input. In *European Conference on Computer Vision*. Springer, 294–310.
- Anthony Talvas, Maud Marchal, Christian Duriez, and Miguel A Otaduy. 2015. Aggregate constraints for virtual manipulation with soft fingers. *IEEE transactions on visualization and computer graphics* 21, 4 (2015), 452–461.

- Bugra Tekin, Federica Bogo, and Marc Pollefeys. 2019. H+ o: Unified egocentric recognition of 3d hand-object poses and interactions. In *Proceedings of the IEEE/CVF conference on computer vision and pattern recognition*. 4511–4520.
- Anastasia Tkach, Mark Pauly, and Andrea Tagliasacchi. 2016. Sphere-meshes for real-time hand modeling and tracking. *ACM Transactions on Graphics (ToG)* 35, 6 (2016), 1–11.
- Dimitrios Tzionas, Luca Ballan, Abhilash Srikantha, Pablo Aponte, Marc Pollefeys, and Juergen Gall. 2016. Capturing hands in action using discriminative salient points and physics simulation. *International Journal of Computer Vision* 118, 2 (2016), 172–193.
- Yangang Wang, Jianyuan Min, Jianjie Zhang, Yebin Liu, Feng Xu, Qionghai Dai, and Jinxiang Chai. 2013. Video-based hand manipulation capture through composite motion control. *ACM Transactions on Graphics (TOG)* 32, 4 (2013), 1–14.
- Zeshi Yang, Kangkang Yin, and Libin Liu. 2022. Learning to use chopsticks in diverse gripping styles. *ACM Transactions on Graphics (TOG)* 41, 4 (2022), 1–17.
- Xinyu Yi, Yuxiao Zhou, Marc Habermann, Soshi Shimada, Vladislav Golyanik, Christian Theobalt, and Feng Xu. 2022. Physical Inertial Poser (PIP): Physics-aware Real-time Human Motion Tracking from Sparse Inertial Sensors. In *IEEE/CVF Conference on Computer Vision and Pattern Recognition (CVPR)*.
- Ri Yu, Hwangpil Park, and Jehee Lee. 2021. Human Dynamics from Monocular Video with Dynamic Camera Movements. *ACM Trans. Graph.* 40 (2021).
- Ye Yuan and Kris Kitani. 2019. Ego-Pose Estimation and Forecasting As Real-Time PD Control. In *2019 IEEE/CVF International Conference on Computer Vision (ICCV)*.
- Ye Yuan, Shih-En Wei, Tomas Simon, Kris Kitani, and Jason Saragih. 2021. SimPoE: Simulated Character Control for 3D Human Pose Estimation. In *Proceedings of the IEEE/CVF Conference on Computer Vision and Pattern Recognition (CVPR)*.
- Petrissa Zell, Bodo Rosenhahn, and Bastian Wandt. 2020. Weakly-supervised Learning of Human Dynamics. In *ECCV*.
- Hao Zhang, Zi-Hao Bo, Jun-Hai Yong, and Feng Xu. 2019. InteractionFusion: real-time reconstruction of hand poses and deformable objects in hand-object interactions. *ACM Transactions on Graphics (TOG)* 38, 4 (2019), 1–11.
- Hao Zhang, Yuxiao Zhou, Yifei Tian, Jun-Hai Yong, and Feng Xu. 2021. Single Depth View Based Real-Time Reconstruction of Hand-Object Interactions. *ACM Transactions on Graphics (TOG)* 40, 3 (2021), 1–12.
- Wenping Zhao, Jianjie Zhang, Jianyuan Min, and Jinxiang Chai. 2013. Robust realtime physics-based motion control for human grasping. *ACM Transactions on Graphics (TOG)* 32, 6 (2013), 1–12.